Research Article Vol. 3, No. 2 / February 2016 / Optica 127

Active temporal and spatial multiplexing of photons

Gabriel J. Mendoza,[1,*] Raffaele Santagati,[1] Jack Munns,[1] Elizabeth Hemsley,[1] Mateusz Piekarek,[1] Enrique Martín-López,[2] Graham D. Marshall,[1] Damien Bonneau,[1] Mark G. Thompson,[1] and Jeremy L. O'Brien[1]

[1]Centre for Quantum Photonics, H. H. Wills Physics Laboratory & Department of Electrical and Electronic Engineering, University of Bristol, Merchant Venturers Building, Woodland Road, Bristol BS8 1UB, UK
[2]Nokia Technologies, Broers Building, 21 J. J. Thomson Avenue, Cambridge CB3 0FA, UK
*Corresponding author: G.Mendoza@bristol.ac.uk

Received 11 August 2015; revised 16 December 2015; accepted 18 December 2015 (Doc. ID 247691); published 29 January 2016

The maturation of many photonic technologies from individual components to next-generation system-level circuits will require exceptional active control of complex states of light. A prime example is in quantum photonic technology: while single-photon processes are often probabilistic, it has been shown in theory that rapid and adaptive feedforward operations are sufficient to enable scalability. Here, we use simple "off-the-shelf" optical components to demonstrate active multiplexing—adaptive rerouting to single modes—of eight single-photon "bins" from a heralded source. Unlike other possible implementations, which can be costly in terms of resources or temporal delays, our new configuration exploits the benefits of both time and space degrees of freedom, enabling a significant increase in the single-photon emission probability. This approach is likely to be employed in future near-deterministic photon multiplexers with expected improvements in integrated quantum photonic technology.

OCIS codes: (270.5290) Photon statistics; (270.5585) Quantum information and processing.

http://dx.doi.org/10.1364/OPTICA.3.000127

1. INTRODUCTION

The active control of light using feedforward/feedback techniques is emerging as an important resource for future large-scale photonic technologies (e.g., [1–3]). In quantum photonics, active control has been understood to have a foundational role since seminal proposals [4,5] have shown rapid and adaptive measurement and feedforward operations as a path to scalability. The benefit of this approach for quantum photonics is the simplicity of the individual components used in the control network—"standard" linear optical elements—as opposed to approaches that require exotic materials or development processes for, e.g., quantum light–matter interfaces [6].

A central challenge in quantum photonics is the nondeterministic nature—probabilistic with a heralded success signal—of single-photon and entangled state generation, which arises from sources based on spontaneous pair generation in nonlinear material (referred to as heralded single-photon sources, or HSPSs) [6] and the negligible interaction between photons [4]. For HSPSs, the maximum theoretical single-photon emission probability is limited to 25% [7], sufficient for small-scale applications and proof-of-principle experiments, but not ultimately scalable in quantum photonic applications requiring many single photons on demand simultaneously. As with other generation processes in quantum photonics with heralded success probabilities well below 50%, (e.g., [8–10]), the success probabilities must be increased above relevant practical thresholds (often well above 50%).

A promising approach to overcome this challenge is to use active optical multiplexing—repeating a nondeterministic generation process in time or space and rerouting to single modes using an adaptive optical switching network (Fig. 1) [11–14]. The individual components used in this approach—switches, delay lines, nonlinear crystals, and single-photon detectors—are generally "off-the-shelf" components that can be acquired commercially today in bulk or fiber, and can conceivably be fabricated into a monolithic integrated chip using standard processes (or with minor modifications) in the near future. With sufficiently high-performance components, active multiplexing can be used to increase the success probabilities of nondeterministic generation processes above relevant thresholds, enabling scalability [15].

Spatial multiplexing [7,11–15] has been successfully implemented with up to four HSPSs [16–19]. While relying fully on spatial multiplexing may be costly in terms of resource requirements [20], temporal multiplexing [21–29] would enable repeated use of the same physical process, reducing resources, system size, and indistinguishability requirements, at the cost of introducing delay lines and reducing the system clock rate. In our view, the most practical large-scale quantum photonic architectures in the future will utilize both spatial and temporal multiplexing to optimize trade-offs between spatial footprint and system clock rate, and other practical considerations (Fig. 1).

Here, we demonstrate the combined operation of active temporal and spatial multiplexing of photons. Using a double-passed

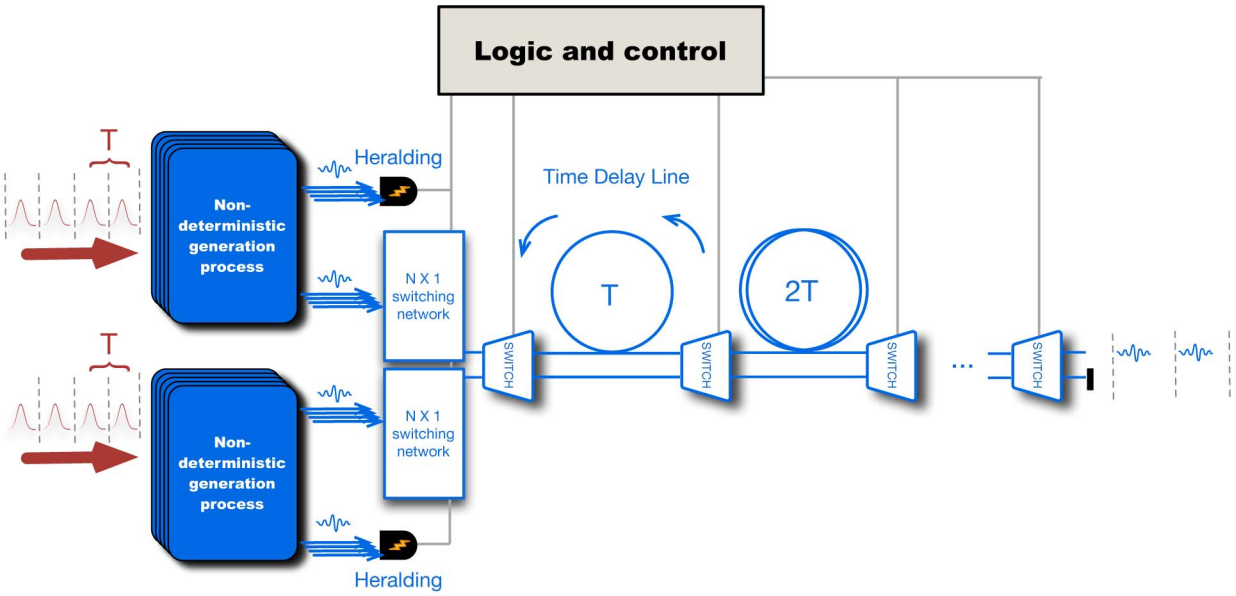

Fig. 1. Future vision of hybrid temporal and spatial multiplexing of photons for large-scale quantum photonics. In spatial multiplexing (left), a nondeterministic generation process is repeated N times in space; on heralded success, an active $N \times 1$ optical switching network will reroute generated photons into specific modes. In temporal multiplexing (right), a nondeterministic generation process is repeated in time with period T; on heralded success, an active optical switching network and delay lines offset photons into output time bins spaced by an integer multiple of the input period and in sync with the system clock cycle. Using both temporal and spatial multiplexing can optimize for resource requirements, spatial footprint, delay line lengths, and clock rate constraints. With sufficiently low-loss switching networks, the generation probability per clock cycle is increased.

HSPS, only a single physical source was used to multiplex eight effective source repetitions, enabling an increase in the heralded photon rate, for a fixed noise level, by up to 76% compared to the same source without multiplexing. Although our demonstration is currently limited by the maximum operation frequency of the switches, our configuration does not rely on components that may be significantly difficult to include in near-future integrated designs, such as quantum light–matter interfaces or polarization modulators, thus showing a configuration well-suited for future development.

2. RESULTS

A. Principle of Operation

In a HSPS, a pulsed laser pumps a nonlinear material, spontaneously generating photon pairs, called signal and idler photons, in a fixed time bin. Assuming a single-mode state [30], the state after passing through the nonlinear material is given by an infinite superposition of Fock state pairs [31]:

$$|\psi\rangle = \sqrt{1-|\xi|^2}\left(|0\rangle_i|0\rangle_s + \sum_{n=1}^{\infty}\xi^n|n\rangle_i|n\rangle_s\right), \quad (1)$$

where i and s are the idler and signal modes and ξ is the squeezing parameter determined by the pump power and the strength of the nonlinearity. Multiphoton pairs generally result in detrimental effects in quantum circuits, necessitating low squeezing parameters so that the single-pair term in Eq. (1) dominates.

Filters are used to separate the signal and idler photons and the pump, and a single-photon detector placed on the idler arm is used to herald the presence of the signal photon. Under ideal conditions and with number-resolving detectors, the theoretical maximum single-photon emission probability of a HSPS is limited to 25% [7], due to the presence of multiphoton pair terms in Eq. (1). While this single-photon emission probability is sufficient for small-scale quantum optics experiments, heralded sources by themselves are not sufficient for scalable quantum technology [15].

A temporal multiplexing technique (also referred to as time multiplexing) [21,22], which uses a HSPS, optical switches, delay line loops, and electronics for feedforward, can be used to boost the single-photon emission probability while keeping the multiphoton contamination low. In this scheme, the HSPS is pumped N times per clock cycle with laser pulses spaced by time T. Signal photons are stored in a long delay line buffer as detection signals from the idler arm are analyzed. When a single photon is heralded in one of the N time bins, a switching network composed of delay line loops (with lengths of integer multiples of T) is driven into a configuration that offsets the photon into a single spatial–temporal mode.

With a sufficient number of time bins per clock cycle, a single-photon pair will be produced in at least one of the time bins with high probability. The probability of heralded single-photon emission from the multiplexed source is approximately (see Supplement 1, Section III for a detailed model)

$$p_{\text{single}}^{\text{MUX}} = \left(1-\left(1-p_{\text{trig}}\right)^N\right)p_{\text{single}}, \quad (2)$$

where p_{trig} is the probability that the HSPS triggers during one time bin and p_{single} is the probability that the triggered emission is a single photon after passing through the lossy switching network [15]. With ideal operation and assuming a lossless switching network, 17 heralded source repetitions enable a source with >99% single-photon emission probability [7], and assuming realistically small losses, ~8–16 heralded source repetitions enable a near-deterministic source with low multiphoton contamination

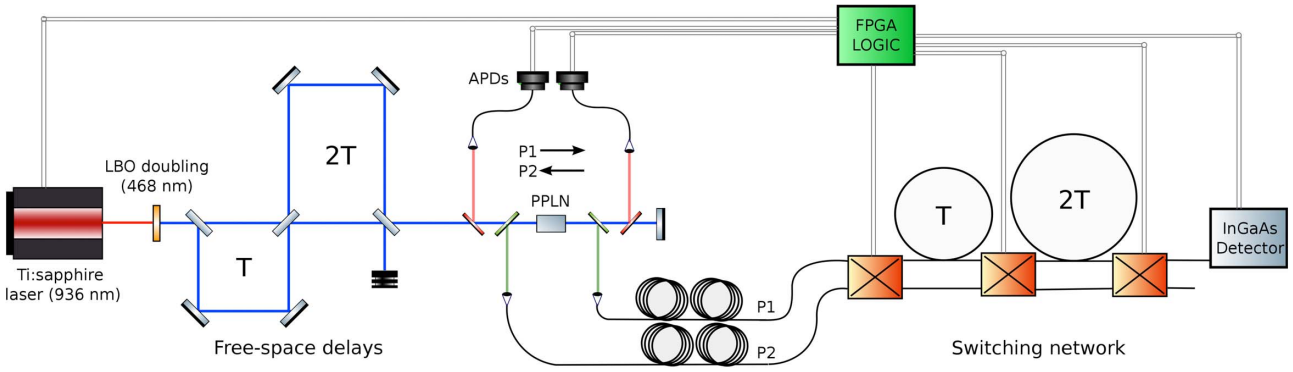

Fig. 2. Experimental setup. Pulses from a femtosecond laser are upconverted using an LBO crystal, split into four copies using free-space delay lines, and passed twice through a PPLN crystal for downconversion. Following separation of the photon pairs and pump using filtering, the heralding signals are analyzed by an oversampling FPGA while the signal photons are stored in long fiber delays. The FPGA configures the switching network to deliver the generated signal photons into a single spatial and temporal mode. P1 and P2 indicate Pass 1 and Pass 2.

(depending on exact experimental parameters) for large-scale applications [15]. Even when considering HSPSs operating with efficiencies far below the theoretical maximum, as is the case with all HSPSs demonstrated to date, multiplexing can still be used to achieve an enhanced heralded single-photon emission probability per clock cycle for a fixed multiphoton contamination probability, offering the possibility of new classes of experiments in the near term.

In this work we implemented a hybrid scheme using two spatially multiplexed sources fed into a temporal multiplexing setup, doubling the number of effective source repetitions (Fig. 2). By using a return pass in the opposite direction through the same nonlinear crystal, hybrid temporal and spatial multiplexing can be implemented with only a single physical source. This scheme enables an additional enhancement to the single-photon emission probability without an additional loss penalty on the generated photons, since the same depth of switches as the temporal multiplexing scheme is used.

B. Implementation

Our experimental setup (Fig. 2) uses a bulk periodically poled lithium niobate (PPLN) downconversion crystal phase matched to produce idler photons at 671 nm and signal photons at 1547 nm from a pump laser at 468 nm. These wavelengths enable high-efficiency detection of the idler photon using silicon avalanche photodiodes (APDs) and low-loss transmission of the signal photon through switches and fiber delay lines.

Each pulse from a pump laser with a 80 MHz repetition rate (12.5 ns pulse spacing) is frequency doubled and split into four pulses spaced by ∼3 ns using a series of free-space delay lines constructed from beam splitters and mirrors. The four pulses then pass through the PPLN crystal and undergo collinear downconversion, probabilistically creating photon pairs in four time bins in the first spatial mode (referred to as Pass 1); a return pass of the pump through the crystal, obtained by recycling the residual pump reflected from a mirror, creates four additional time bins in a separate spatial mode (Pass 2). For each pass, the four effective sources passively delayed in time are referred to as "Delays," e.g., Pass 1, Delay 3. The spectra of the signal photons from different delays of the same pass were shown to have a high degree of similarity (mean of 97.9 ± 1.8%, see Supplement 1, Section II), and moderate similarity between the two different passes (mean of 92.8 ± 5.2%, see Supplement 1, Section II). Furthermore, an in-line polarizer was used to verify that the photons emitted from each source had identical polarization.

The polarization-maintaining, active optical switching network (see Appendix A: Methods) is composed of low-loss fiber switches (∼1 dB loss per switch, 500 kHz maximum operation frequency) and two fiber delay loops matched to the free-space delay lines (see Fig. 2) [21]. Detection signal rising edges, which can fall in any of the four closely spaced time bins, are correctly discriminated using a fast oversampling field programmable gate array (FPGA) (see Appendix A: Methods), which then configures the switches for feedforward multiplexing of the eight time and spatial modes. To avoid driving the switches faster than their maximum operation frequency, an asynchronous "idle time" of 2 μs was programmed into the FPGA to limit the rate of detected heralding signals. During heralding detection, feedforward processing, and switch configuration, the signal photons are stored in long delay lines of telecom fiber. Signal photons are detected using an InGaAs detector, gated from the idler photon detection events.

C. Measured Photon Statistics from Multiplexed and Nonmultiplexed Sources

Photon counting statistics were collected for the eight nonmultiplexed sources and the multiplexed source. These included triggering (idler singles) rates, heralded signal photon (coincidence) rates, and accidental rates (see Appendix A: Methods for collection methods and Supplement 1, Section I for the full data and analysis). For all coincidence and accidental measurements, time-averaged dark counts in the signal arm, which did not have a significant dead-time effect, were subtracted from the totals in order to isolate the effect of dark count accidentals from those due to multiphoton contamination. This also allows for an examination of single-photon *emission* probabilities from the sources, rather than also including additional effects due to detection at the end of the circuit, which may have different characteristics for different applications. The data was found to be in excellent agreement with our model of the nonmultiplexed and multiplexed sources (see Supplement 1, Section III).

The key measure of performance for our multiplexed source is the heralded photon rate for a fixed coincidence-to-accidental ratio (CAR). The CAR serves as a measure of noise due to single-photon emission and multiphoton contamination probabilities;

this measure of noise cannot be inferred from coincidence rates alone. The heralded photon rates for fixed CAR for the 8 × multiplexed and nonmultiplexed sources are plotted in Fig. 3 (data from the 4 × multiplexed source is shown in Supplement 1, Section I). At high pump powers, corresponding to low CARS, the rates of coincidences for the multiplexed sources were suppressed due to the saturation of triggering events, as predicted by our model (Supplement 1, Section III). For a fixed CAR, in the regime where saturation effects are small, the 4 × multiplexed source did not show a significant increase in the heralded photon rate, and was limited mainly by the loss of the switching network (∼4 dB loss for each path). However, the 8 × multiplexed source exhibited an increased heralded photon rate between 33% and 59%, for the same CAR, over the best nonmultiplexed source, and between 47% and 76% over the mean from the nonmultiplexed sources (Pass 1 only), demonstrating a direct improvement [Fig. 3(b)]. In our model we corrected for the effects of extrinsic loss on the rate of heralded photon production [dashed line Fig. 3(a), see Appendix A and Supplement 1, Section III], indicating a potential improvement of ∼114% for a wide range of CAR values compared to the expected heralded photon rate from the nonmultiplexed sources (also with extrinsic loss removed). This enhancement can be mapped to a comparable increase in the single-photon emission probability for a fixed multiphoton emission probability (see Supplement 1, Section IV).

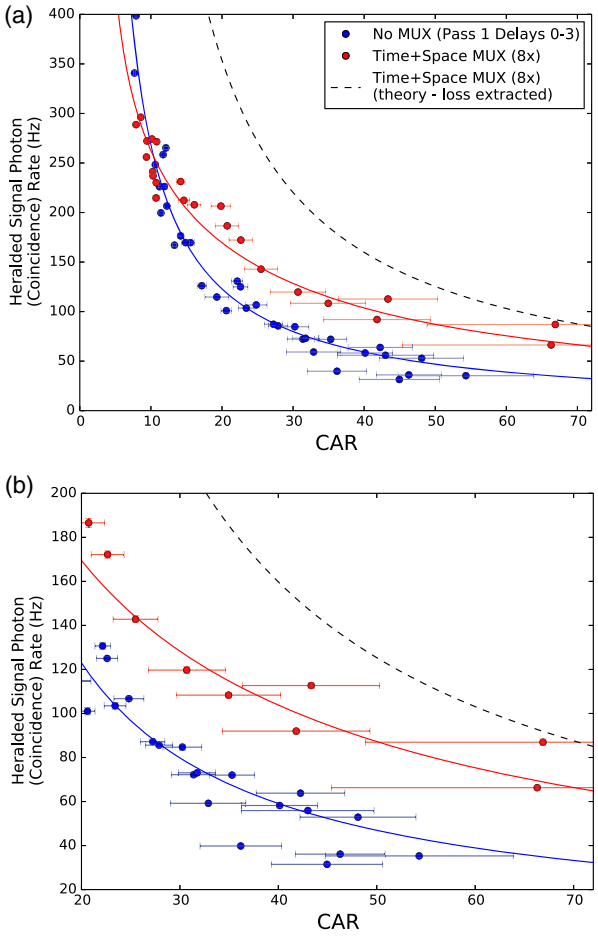

Fig. 3. Heralded signal photon (coincidence) rate versus CAR for multiplexed and nonmultiplexed sources. (a) The full dataset, and (b) detail at low powers, where saturation effects due to electronics are small. "Delays 0–3" refers to the four effective nonmultiplexed sources passively delayed in time. Red points are for the 8 × multiplexed source, and blue points are for the nonmultiplexed sources (Pass 1). Solid lines are based on a theory fit using measured parameters. Dashed line shows a potential improvement using a correction for extrinsic sources of loss based on the theory model.

3. DISCUSSION

We demonstrated temporal and spatial multiplexing of eight photon bins in a hybrid setup to enhance the heralded photon emission statistics compared to nonmultiplexed sources. Although our demonstrated improvement was limited by the maximum operation frequency of the switches, we note that even low-rate high-efficiency multiplexed sources will likely find applications in the near term, due to the increased single-photon generation probability per clock cycle. Therefore, a possible solution is to use a pulse picker to limit the repetition rate of the laser source to the maximum operation frequency of the switches. Combined with single-photon detectors with near-unity efficiency and low dark counts at telecom wavelengths (e.g., [32]), the configuration demonstrated here will provide a practical advantage for single-photon generation in future experiments. Ultimately, multiplexed sources with the highest single-photon emission rates will require the development of a lower-loss high-speed optical switch (recent, promising prototypes include Kerr effect [33] and electro-optic-based [34] switches). Driven by the demand for high-performance modulation and switching for classical photonics applications (see, e.g., [35]), breakthroughs in this area are expected in the coming years.

Although the focus of our current demonstration was not on optimizing photon indistinguishability, we expect that small adjustments to our setup, such as passing the pump beam through a spatial pinhole filter at the inputs of the source, will improve this aspect in the future (see Supplement 1, Section II). In our multiplexed source, photons from different delays had similar spectral properties, identical polarizations, and similar source efficiencies and couplings. Our setup of adjustable free-space delays allows for the fine-tuning of the temporal delays of the photons to within a coherence length, indicating that photon interference between two of our multiplexed sources, up to the intrinsic limit of the PPLN sources themselves, should be possible. In future implementations, waveguide single-photon sources (e.g., [36]) are also compatible with our setup to further improve photon indistinguishability and reduce mode mismatch.

Temporal multiplexing techniques will almost certainly be required in future large-scale quantum photonic circuits in order to substantially reduce resource requirements. Furthermore, hybrid temporal and spatial multiplexing will be important in order to balance trade-offs among resource requirements, spatial footprint, and temporal delays. Integrated photonic components, including photon pair sources (e.g., [37]), switches (e.g., [38]), filters (e.g., [39]), delay lines (e.g., [40]), and detectors (e.g., [32]), are under development. Scaling down our setup will enable a multiplexing template capable of realizing new classes of quantum photonics technology, as well as provide useful tools for high-performance active optical control.

APPENDIX A: METHODS

1. Experimental Setup

A mode-locked, Ti:sapphire laser (Tsunami, Spectra Physics) produced ∼150 fs pulses at 936 nm; a LBO crystal (Newlight) was

used to frequency convert to 468 nm. To enable low-loss, near 50–50 splitting of the pulsed pump beam, laser line nonpolarizing beam splitters (Newport) were used in the free-space delays. The PPLN crystal (Covesion) was 3 mm long and phase-matched at 110°C using an oven and temperature controller. Dichroic mirrors (Semrock) were used to separate the signal and idler photons from the pump, and Pellin–Broca prisms were used for further spatial filtering. A bandpass filter with FWHM of ∼2.6 nm and center at 671 nm (Semrock) was used on the idler arms of each pass for further filtering.

Polarization-maintaining switches (Agiltron, ∼1 dB loss per switch, 500 kHz max operation frequency) were based on an electro-optic material. Standard telecom fiber was used for the long delay buffer (∼200 m, ∼90% transmission) and polarization-maintaining low-dispersion fiber (Corning) was used for the variable delay line loops (∼0.65 m and 1.30 m, ∼95% transmission). Fiber polarization controllers (Fiberpro) were used before the polarization-maintaining switching network to match the polarizations of photons from the two passes. To enable reliable comparison between multiplexed and nonmultiplexed source measurements, a MEMS switch with nearly balanced loss was used to route the photons into or around the multiplexing switch network.

2. Photon Detection

Idler (triggering) photons were detected using silicon APDs (PerkinElmer, ∼65% efficiency). Pump leakage and dark counts on the idler arms were found to be negligible (∼500 Hz) compared to the triggering rates.

Idler photon detection signals were discriminated with an oversampling FPGA (Xilinx Spartan 6) using internal delays and a 80 MHz, "locked-to-clock" reference input from the Ti:sapphire laser. The FPGA was designed so that, after signal detection, an "idle time" of 2 μs became active to avoid further detection. For every detected signal (regardless of time bin), a gating signal was output with a constant delay with reference to the original input clock, to ensure correct heralding of the temporally multiplexed photons. The total (unoptimized) internal delay of the FPGA logic was ∼60 ns.

Signal photons were detected using InGaAs detectors (ID Quantique, ∼25% efficiency). Coincidence counts, joint detection between idler and signal photons from paired generation events, were collected using gated detection of the signal photon from idler detection signals from the FPGA. Accidental counts, joint detection between idler and gated signal photons from unpaired generation events, were then collected by shifting the temporal delay of the FPGA input clock by a multiple of the clock cycle. Pump leakage in the signal arms was found to be negligible at the measured powers. Dark counts detected by the InGaAs detectors (in the regime of 5%–10% of the heralded coincidence counts in gated mode) were measured by blocking the signal arm path; these time-averaged counts were then subtracted from the count totals. The gate width used was 1.8 ns.

3. Extrinsic Sources of Loss

Extrinsic sources of loss in the setup include the following. (1) Loss due to measurement apparatus: a small amount of extra loss (4%) on the multiplexed source was due to asymmetric loss of the MEMS switch used to switch between multiplexing and nonmultiplexing channels for measurement. (2) Loss due to the deadtime of available electronic amplifiers: the two electronic amplifiers used to amplify the signal from the APD and into the FPGA have deadtimes of ∼0.1 μs, resulting in missed pulses from the APD. In principle, much faster amplifiers with negligible deadtimes can be used to eliminate this source of loss. (3) Loss due to the limited switch repetition rate (500 kHz). An asynchronous "idle time" of 2 μs was programmed into the FPGA to avoid driving the switches faster than their 500 kHz maximum operation frequency. The switch repetition rate is set by the switch driver board; the switches themselves have a faster intrinsic rise and fall time, with maximum extinction ratio, of 300 ns (∼3 MHz).

Funding. Engineering and Physical Sciences Research Council (EPSRC); European Research Council (ERC); PICQUE; BBOI; U.S. Army Research Office (ARO) (W911NF-14-1-0133); Air Force Office of Scientific Research (AFOSR); Royal Society Wolfson Merit Award; Royal Academy of Engineering Chair in Emerging Technologies; FP7 Marie Curie International Incoming Fellowship scheme.

Acknowledgment. We thank Xiao Ai, Daryl Beggs, Allison Rubenok, Gary Sinclair, Ivo Straka, Jianwei Wang, Andrew Young, and Xiou-Qi Zhou for useful discussions and assistance.

See Supplement 1 for supporting content.

REFERENCES

1. F. Morichetti, S. Grillanda, and A. Melloni, "Breakthroughs in photonics 2013: toward feedback-controlled integrated photonics," IEEE Photon. J. **6**, 1–6 (2014).
2. R. Hamerly and H. Mabuchi, "Advantages of coherent feedback for cooling quantum oscillators," Phys. Rev. Lett. **109**, 173602 (2012).
3. N. Tezak and H. Mabuchi, "A coherent perceptron for all-optical learning," EPJ Quantum Technol. **2**, 10 (2015).
4. E. Knill, R. Laflamme, and G. J. Milburn, "A scheme for efficient quantum computation with linear optics," Nature **409**, 46–52 (2001).
5. D. E. Browne and T. Rudolph, "Resource-efficient linear optical quantum computation," Phys. Rev. Lett. **95**, 010501 (2005).
6. M. D. Eisaman, J. Fan, A. Migdall, and S. V. Polyakov, "Single-photon sources and detectors," Rev. Sci. Instrum. **82**, 071101 (2011).
7. A. Christ and C. Silberhorn, "Limits on the deterministic creation of pure single-photon states using parametric down-conversion," Phys. Rev. A **85**, 023829 (2012).
8. Q. Zhang, X. H. Bao, C. Y. Lu, X. Q. Zhou, T. Yang, T. Rudolph, and J. W. Pan, "Demonstration of a scheme for the generation of event-ready entangled photon pairs from a single-photon source," Phys. Rev. A **77**, 062316 (2008).
9. M. Varnava, D. Browne, and T. Rudolph, "How good must single photon sources and detectors be for efficient linear optical quantum computation?" Phys. Rev. Lett. **100**, 060502 (2008).
10. H. Cable and J. Dowling, "Efficient generation of large number-path entanglement using only linear optics and feed-forward," Phys. Rev. Lett. **99**, 163604 (2007).
11. A. L. Migdall, D. Branning, and S. Castelletto, "Tailoring single-photon and multiphoton probabilities of a single-photon on-demand source," Phys. Rev. A **66**, 053805 (2002).
12. J. H. Shapiro and F. N. Wong, "On-demand single-photon generation using a modular array of parametric downconverters with electro-optic polarization controls," Opt. Lett. **32**, 2698–2700 (2007).
13. T. Jennewein, M. Barbieri, and A. G. White, "Single-photon device requirements for operating linear optics quantum computing outside the post-selection basis," J. Mod. Opt. **58**, 276–287 (2011).
14. M. G. Segovia, P. Shadbolt, D. E. Browne, and T. Rudolph, "From three-photon GHZ states to universal ballistic quantum computation," Phys. Rev. Lett. **115**, 020502 (2015).

15. D. Bonneau, G. J. Mendoza, J. L. O'Brien, and M. G. Thompson, "Effect of loss on multiplexed single-photon sources," New J. Phys. **17**, 043057 (2015).
16. X. Ma, S. Zotter, J. Kofler, T. Jennewein, and A. Zeilinger, "Experimental generation of single photons via active multiplexing," Phys. Rev. A **83**, 043814 (2011).
17. M. J. Collins, C. Xiong, I. H. Rey, T. D. Vo, J. He, S. Shahnia, C. Reardon, T. F. Krauss, M. J. Steel, A. S. Clark, and B. J. Eggleton, "Integrated spatial multiplexing of heralded single-photon sources," Nat. Commun. **4**, 2582 (2013).
18. T. Meany, L. A. Ngah, M. J. Collins, A. S. Clark, R. J. Williams, B. J. Eggleton, M. J. Steel, M. J. Withford, O. Alibart, and S. Tanzilli, "Hybrid photonic circuit for multiplexed heralded single photons," Laser Photon. Rev. **8**, L42–L46 (2014).
19. C. Xiong, T. D. Vo, M. J. Collins, J. Li, T. F. Krauss, M. J. Steel, A. S. Clark, and B. J. Eggleton, "Bidirectional multiplexing of heralded single photons from a silicon chip," Opt. Lett. **38**, 5176–5179 (2013).
20. Y. Li, P. C. Humphreys, G. J. Mendoza, and S. C. Benjamin, "Resource costs for fault-tolerant linear optical quantum computing," Phys. Rev. X **5**, 041007 (2015).
21. J. Mower and D. Englund, "Efficient generation of single and entangled photons on a silicon photonic integrated chip," Phys. Rev. A **84**, 052326 (2011).
22. C. T. Schmiegelow and M. A. Larotonda, "Multiplexing photons with a binary division strategy," Appl. Phys. B **116**, 447–454 (2013).
23. T. B. Pittman, M. J. Fitch, B. C. Jacobs, and J. D. Franson, "Periodic single-photon source and quantum memory," Proc. SPIE **5161**, 57–65 (2004).
24. P. P. Rohde, L. G. Helt, M. J. Steel, and A. Gilchrist, "Multiplexed single-photon state preparation using a fibre-loop architecture," Phys. Rev. A **92**, 053829 (2015).
25. R. J. A. Francis-Jones and P. J. Mosley, "Temporal loop multiplexing: a resource efficient scheme for multiplexed photon-pair sources," arXiv:1503.06178 (2015).
26. K. T. McCusker and P. G. Kwiat, "Efficient optical quantum state engineering," Phys. Rev. Lett. **103**, 163602 (2009).
27. K. R. Motes, A. Gilchrist, J. P. Dowling, and P. P. Rohde, "Scalable boson-sampling with time-bin encoding using a loop-based architecture," Phys. Rev. Lett. **113**, 120501 (2014).
28. M. A. Broome, M. P. Almeida, A. Fedrizzi, and A. G. White, "Reducing multi-photon rates in pulsed down-conversion by temporal multiplexing," Opt. Express **19**, 22698–22708 (2011).
29. P. P. Rohde, "Simple scheme for universal linear-optics quantum computing with constant experimental complexity using fiber loops," Phys. Rev. A **91**, 012306 (2015).
30. W. Grice, A. U'Ren, and I. Walmsley, "Eliminating frequency and space-time correlations in multiphoton states," Phys. Rev. A **64**, 063815 (2001).
31. C. Gerry and P. Knight, *Introductory Quantum Optics* (Cambridge University, 2004).
32. F. Marsili, V. B. Verma, J. A. Stern, S. Harrington, A. E. Lita, T. Gerrits, I. Vayshenker, B. Baek, M. D. Shaw, R. P. Mirin, and S. W. Nam, "Detecting single infrared photons with 93% system efficiency," Nat. Photonics **7**, 210–214 (2013).
33. T. M. Rambo, K. McCuster, Y. Huang, and P. Kumar, "Low-loss all-optical quantum switching," in *IEEE Photonics Society Summer Topical Meeting Series* (IEEE, 2013), pp. 179–180.
34. A. Rao, A. Patil, J. Chiles, M. Malinowski, S. Novak, K. Richardson, P. Rabiei, and S. Fathpour, "Heterogeneous microring and Mach-Zehnder lithium niobate electro-optical modulators on silicon," in *Conference on Lasers and Electro-Optics (CLEO)*, OSA Technical Digest (Optical Society of America, 2015), paper STu2F-4.
35. D. Moss, R. Morandotti, A. L. Gaeta, and M. Lipson, "New CMOS-compatible platforms based on silicon nitride and Hydex for nonlinear optics," Nat. Photonics **7**, 597–607 (2013).
36. P. Aboussouan, O. Alibart, D. B. Ostrowsky, P. Baldi, and S. Tanzilli, "High-visibility two-photon interference at a telecom wavelength using picosecond-regime separated sources," Phys. Rev. A **81**, 021801 (2010).
37. J. Silverstone, D. Bonneau, K. Ohira, N. Suzuki, H. Yoshida, N. Iizuka, M. Ezaki, C. M. Natarajan, M. G. Tanner, R. H. Hadfield, V. Zwiller, G. D. Marshall, J. G. Rarity, J. L. O'Brien, and M. G. Thompson, "On-chip quantum interference between silicon photon-pair sources," Nat. Photonics **8**, 104–108 (2014).
38. C. Lacava, M. J. Strain, P. Minzioni, I. Cristiani, and M. Sorel, "Integrated nonlinear Mach Zehnder for 40 Gbit/s all-optical switching," Opt. Express **21**, 21587–21595 (2013).
39. S. H. Jeong, D. Shimura, T. Simoyama, M. Seki, N. Yokoyama, M. Ohtsuka, K. Koshino, T. Horikawa, Y. Tanaka, and K. Morito, "Low-loss, flat-topped and spectrally uniform silicon-nanowire-based 5th-order CROW fabricated by ArF-immersion lithography process on a 300-mm SOI wafer," Opt. Express **21**, 30163–30174 (2013).
40. H. Lee, T. Chen, J. Li, O. Painter, and K. J. Vahala, "Ultra-low-loss optical delay line on a silicon chip," Nat. Commun. **3**, 867 (2012).